ADSORPTION OF SIMPLE AND COMPLEX FLUIDS ON NON-GRAPHITIZED CARBON BLACK AND ACTIVATED CARBON – TRANSITION FROM SUB-CRITICAL TO SUPERCRITICAL ADSORPTION AND A NEW METHOD TO DETERMINE PORE SIZE DISTRIBUTION OF ACTIVATED CARBON

D. D. Do, G. Birkett and H. Do, Dept. of Chemical Engineering, University of Queensland, St. Lucia, Qld 4072, Australia

Abstract

Description of adsorption on carbonaceous surfaces and in porous carbon requires first a thorough understanding of adsorption of simple and complex gases on a homogeneous graphite surface. The relative homogeneity of the surface of a highly graphitized carbon black makes it a perfect model to test the potential of any adsorption model for its capability in the prediction of adsorption in more complicated carbon structure. By starting with perfect homogeneous surface allows one to delineate the surface effects from the others such as the confinement effects, the defects on the surface and the effects of impurities (functional groups). The test of adsorption model for graphitized thermal carbon black is aided with the numerous excellent data in the literature for simple as well as complex gases. Among the many adsorption models that have been proposed in the literature, the ones that have foundation in molecular interactions are the best in terms of probing the molecular origins of adsorption. In this talk I will concentrate on the molecular models using Monte Carlo simulation as this is more suitable than others (such as density functional theory and molecular dynamics) in obtaining information on adsorption equilibria. The adsorption molecular models require mainly the detailed information of interaction between molecules, and if that information is accurately available the Monte Carlo simulation should provide a full description of adsorption. We will test this assertion with adsorption of noble gases first, and although the description of isotherm is reasonably adequate we still need to consider in a subtle manner the way how the surface would interact with fluid particles and the way how the surface would influence the interactions among the fluid particles. This surface influence will then be studied with some complex fluids, and I will illustrate this with some commonly used gases, such as nitrogen, carbon tetrachloride and benzene. Complex gases tend to show a reasonably complex behaviour in adsorption isotherm and isosteric heat. Finally I will consider the strongly associating fluids such as those exhibiting strong hydrogen bonding, for example water, methanol and ammonia. Their adsorption behaviour is drastically different from that of simple fluids, and with the use of molecular simulation we are able to have a deeper insight into the way how molecules interact with the surface. The strong association of fluid particles highlight the significance of functional groups (or impurities), no matter how low the concentration of the functional group is. These functional groups are undetectable with the use of simple fluids. The association between fluid particles is competing against the association between the functional group and the fluid particle, and in this respect, the adsorption isotherm and the isosteric heat behave differently from those observed with simple gases. Next, the various aspects of adsorption under supercritical conditions will be highlighted with the aid of molecular simulation.

Once we understand how fluids behave on a homogeneous graphite surface, I will discuss how adsorption is affected when surface has defects. A model for defective surface is developed for non-graphitized carbon black, and it has been shown that this model can describe reasonably well the various features of carbon black with varying degrees of graphitization. Finally I talk about the pore size distribution and present a new method to derive the pore size distribution.

1. Introduction

Production of new carbon materials is an area of intensive investigation in recent years and in parallel with this has been the research to further understand the mechanisms of adsorption of gases in these materials. Separation of competing factors underlying the adsorption can be quite complex, and to this end it becomes necessary to study adsorption on the simplest surfaces in order to justify the adsorption models, among which the ones that have basis in molecular interactions are the most useful. Here we take graphite as the reference surface to test the potential of these molecular adsorption models. The widespread application of these models has stemmed from the greater speed of today personal computer and the development of potential models for wider range of adsorbates. We will address a number of factors affecting adsorption, for example, the surface mediation, the adsorbate shape and charges, and temperature.

2. Simulation and Potential Equations

There are a number of molecular simulation tools that are available in the literature, density functional theory, molecular dynamics and Monte Carlo simulation. The latter is the most versatile in investigating the adsorption equilibria, and this is what we will present here. Central to all molecular simulation method is the development of potential equations.

2.1 Fluid Potentials

Adsorbates used in this work can be modelled by potential equations that involve dispersive sites and fixed charges. The interaction between dispersive sites is described by the 12-6 Lennard-Jones equation while that between charges is described by the Coulomb equation. Thus one can write the potential energy of interaction between molecule *i* and molecule *j*:

$$\varphi_{ij} = \sum_{a=1}^{A}\sum_{b=1}^{B}\frac{q_i^a q_j^b}{4\pi\varepsilon_0 r_{ij}^{ab}} + \sum_{c=1}^{C}\sum_{d=1}^{D}4\varepsilon_{ij}^{cd}\left[\left(\frac{\sigma_{ij}^{cd}}{r_{ij}^{cd}}\right)^{12} - \left(\frac{\sigma_{ij}^{cd}}{r_{ij}^{cd}}\right)^{6}\right]$$

The cross parameters are calculated from the usual Lorentz-Berthelot rule. Usually we correct the cross-well depth of interaction energy with a factor F to account for the deviation from this rule.

2.2 Surface Potential

Potential energy of interaction between a fluid particle and a surface can be obtained by summing all the pairwise interaction energy between the fluid particle and each of the solid atoms. For a homogeneous surface such as graphite, we usually treat it as a continuum with a constant surface density, and in this case the Steele 10-4-3 equation (1973) is used:

$$\varphi_{i,s} = \sum_{a=1}^{A} 2\pi\rho_s\varepsilon_{is}^a\left(\sigma_{is}^a\right)^2\left[\frac{2}{5}\left(\frac{\sigma_{is}^a}{z_i^a}\right)^{10} - \left(\frac{\sigma_{is}^a}{z_i^a}\right)^4 - \left(\frac{{\sigma_{is}^a}^4}{3\Delta\left(z_i^a + 0.61\Delta\right)^3}\right)\right]$$

where ρ_s is the carbon surface density, and Δ is the separation distance between graphite layers. In the case of slit pores whose walls are treated as Steele surface, the potential energy is simply the sum of those contributed by both walls.

2.3 Functional Groups

Carbon surfaces contain various functional groups which are attached to the graphene surface mainly at the edges. Some of the common functional groups are carbonyl, carboxyl and hydroxyl groups (Birkett and Do, 2007). The configuration of functional groups strongly affects the adsorption isotherms and isosteric heats of water, ammonia and ethanol and methanol.

2.4 Simulation Methodology

Monte Carlo simulations were conducted using the grand canonical (GCMC) ensemble. This is the natural choice for simulation studies since, for this ensemble, the temperature, volume and chemical potential of the system are specified. The output of the simulation is the density, and the plot of this density versus chemical potential (or pressure via appropriate equation of state) is the simulated adsorption isotherm. This can be compared with experimental data. Since isosteric heat data are also available in the literature it is also useful to compare it with the simulated isosteric heat given below:

$$q_{st} \cong \frac{\langle NU\rangle - \langle N\rangle\langle U\rangle}{\langle N^2\rangle - \langle N\rangle\langle N\rangle} + kT$$

in which we have assumed ideal gas law and the adsorbed molar volume is smaller than the bulk gas molar volume. This heat can be broken down to three contributions, one due to solid-fluid interaction, the others to fluid-fluid interaction and fluid-functional group interaction.

3. Noble Gases Adsorption on Graphite

3.1 Argon

Argon adsorption on graphite is perhaps the simplest system to study, and its intensive experimental data (Avgul and Kiselev, 1970; Gardner et al., 2001) is useful to justify any molecular adsorption model. With the widely used molecular parameters of argon (σ = 3.405 A; ε/k = 119.8 K), the following figure (Figure 1a) shows the simulated isotherm as solid line. Also presented in the figure are experimental data shown as symbols. The agreement between the two is regarded as good, with an exception that during the approach of the monolayer the deviation is quite significant. So what is the cause of this deviation? One possible explanation to this is that when the monolayer is approached, particles are getting closer to each other and their interactions are not the same as those when they are in the bulk phase (which is isotropic). In the case of adsorption, the situation is no longer isotropic and therefore the molecular properties of particles close to the surface should be affected by it. The microscopic reason for this influence could be explained as follows. The surface could polarize the particles and hence create an induced dipole in each particle. The presence of these induced dipoles then gives rise to a reduction in the intermolecular interaction energy between the fluid particles (Do and Do, 2007a). This approach of explicit consideration of induced dipoles is quite cumbersome in computation, and it is useful to develop a simpler means for describing this reduction in fluid-fluid potential energy. This has been presented by Do and co-workers (2004-2006). They introduced the following equation, $\varphi_{i,j}^{eff} = g\,\varphi_{i,j}$, where g is the damping factor, and we argue that this factor is a direct function of the polarizability of the fluid particle. We suggest an empirical equation for this damping factor, $g = \exp(-\chi\varepsilon_{ij,s}/kT)$, where χ is called the damping constant. By accounting for this factor, we can describe the isotherm very accurately as seen in Figure 1b (Do and Do, 2005b).

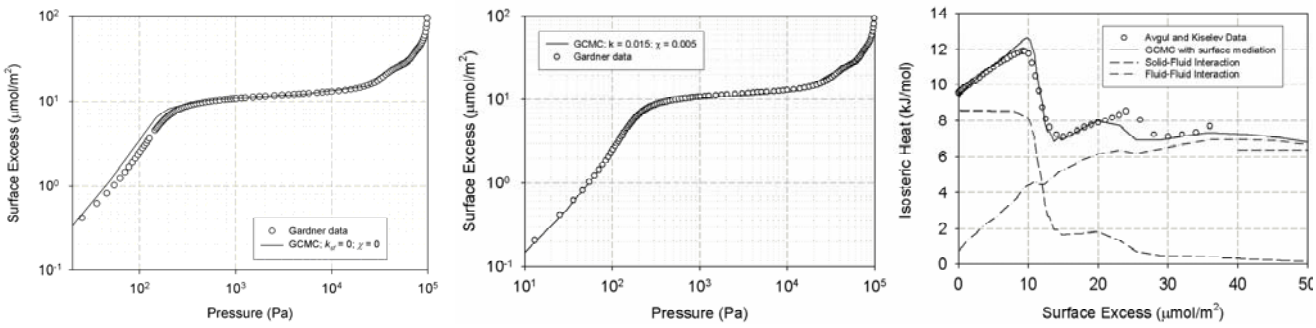

Figure 1. Simulated adsorption isotherm (solid line) and the experimental data (symbols) for argon on GTCB at 87.3 K.

The molecular adsorption model, with the allowance for the surface mediation, can describe well the data, not only at 87.3 K but also at other temperatures. For this model to have credibility, it should describe heat of adsorption, and it, indeed, is as shown in Figure 1c. We have also shown this success with other noble gases as well, and found that the damping constant is a linear function of polarizability, illustrating the possibility of polarization of particle by the electric field of the surface.

4. Non-Polar Gas Adsorption

4.1 Methane

Only noble gases have spherical geometry (in its strict sense). Methane has a tetrahedral shape, but fortunately the hydrogen atom does not have strong interaction energy as the carbon atom it can be practically regarded as a sphere, at least for not very dense systems. For a solid phase, the shape might become important, but we shall not be concerned with solid phase here. The bulk phase behaviour of methane has been shown to be described well with a single site LJ model. Using this potential model in adsorption of methane on graphite, we obtain an excellent description of adsorption isotherm (Do and Do, 2006d). Even when we use a five-site model to simulate adsorption, we do not detect any difference between the simulation results using 5-site and 1-site models. This confirms the adequacy in treating methane as a sphere in adsorption.

4.2 Carbon Tetrachloride

We see that a molecule of tetrahedral shape, like methane, can be described by a single site model. Is this true for other molecules having the same shape? Let us test this with carbon tetrachloride. Figure 2a shows the description of adsorption isotherm with the various 1-site potential models. Clearly the description is poor. What are the reasons for this and why one species can be described well by 1-site model and the others can not? The answer lies in the fact that in the case of carbon tetrachloride, the chlorine atom has a higher interaction energy than the central carbon atom, and therefore the shape of carbon tetrachloride becomes a significant factor. The implication of this high energy chlorine compared to carbon is that when one carbon tetrachloride is adsorbed on a graphite surface, it will sit on this surface as a tripod configuration which maximizes the interaction. This is indeed the case because when we use the 5-site model to model carbon tetrachloride we get a much better description of the adsorption isotherm (solid line in Figure 2b). The surface mediation is also accounted in that when two carbon tetrachloride molecules are close to the surface, the fluid-fluid interaction has to be reduced by 5% and this is possibly due to the polarization of chlorine atoms caused by the electric field exerted by the surface (Do and Do, 2006b). The good description of carbon tetrachloride adsorption with a 5-site model is also observed at other temperatures, and like noble gases the description of isosteric heat versus loading by our model is also very good as shown in Figure 2c.

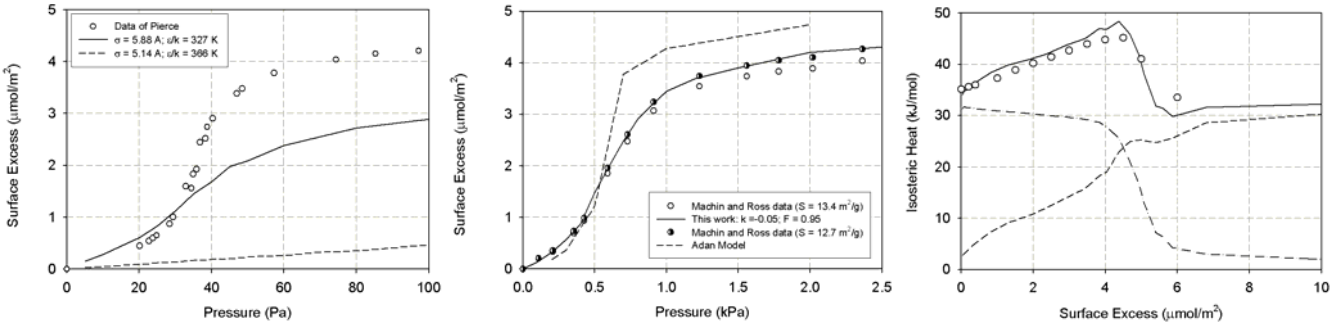

Figure 2 (a) Adsorption isotherm of carbon tetrachloride at 273 K (circle symbols: experimental data; solid line: GCMC results); **(b)** Adsorption isotherm of carbon tetrachloride on GTCB at 323K; **(c)** The isosteric heat versus loading (Circle symbols: Experimental data; solid-line: GCMC simulation results; dashed-dotted line: contribution of solid-fluid to the isosteric heat; dashed line: contribution of fluid-fluid to the isosteric heat)

The configuration of carbon tetrachloride adsorption can be studied by plotting the local density versus distance above the surface and the angle formed between the vector joining the carbon atom and one of the chlorine atoms and the normal vector to the surface. This is shown in Figure 3a for P = 40 Pa, at which about 70% of the surface is covered with carbon tetrachloride molecules. It is clear that most of these molecules take a tripod configuration (angle 0) and the remaining adopts a slant configuration with an angle of 2 radians. The tripod configuration is energetic favourable while the slant configuration of 2 radians is possible to balance the energetic factor and the entropic factor with the latter to mean that more carbon tetrachloride molecules could be packed into the first layer.

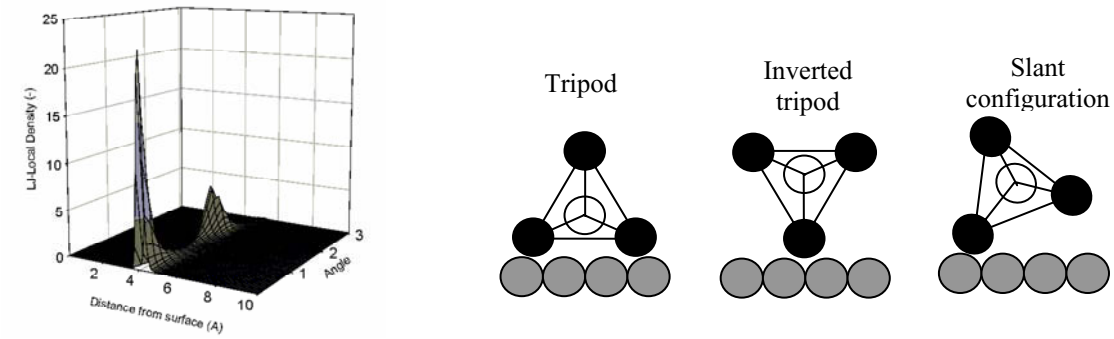

Figure 3: 3D-local density distribution versus distance from the surface and the angle θ

4.3 Benzene

We have seen the influence of shape in the adsorption of relatively simple molecules such as carbon tetrachloride. The difference between this and other simpler fluids is the way carbon tetrachloride molecules pack in the monolayer. The behaviour of isosteric heat is somewhat similar to simpler gases, although in the case of carbon tetrachloride we observe the modest decrease in the solid-fluid contribution to the isosteric heat (dashed line in Figure 2c) in the region of sub-monolayer coverage. This is due to the greater contribution of the slant configuration of carbon tetrachloride as loading is increased. We now consider benzene adsorption on graphite, and this is an interesting case because the isosteric heat versus loading is practically constant in the sub-monolayer coverage. This is in stark contrast to the cases that we have dealt with thus far.

There are a number of potential models that have been proposed in the literature for benzene. The one proposed by Wick et al. (2002) is the most suitable as it can describe vapour-liquid equilibrium well. It has six dispersive sites and three partial charges placed along the axis that runs perpendicular through the ring. Experimental data of isotherm and isosteric heat at 293 K are available from Isirikyan and Kiselev (1961). By accounting for the surface mediation, the adsorption isotherm is described well by the simulation results (Do and Do, 2006a). This is shown in Figure 4a as solid line, and also shown in the figure are the simulation results where no surface mediation is accounted for (dashed line). One thing to note here is that the surface mediation of benzene is stronger for benzene than carbon tetrachloride. Whenever two benzene molecules are in the first layer, the fluid-fluid interaction is reduced by 10%, compared to 5% in the case of carbon tetrachloride.

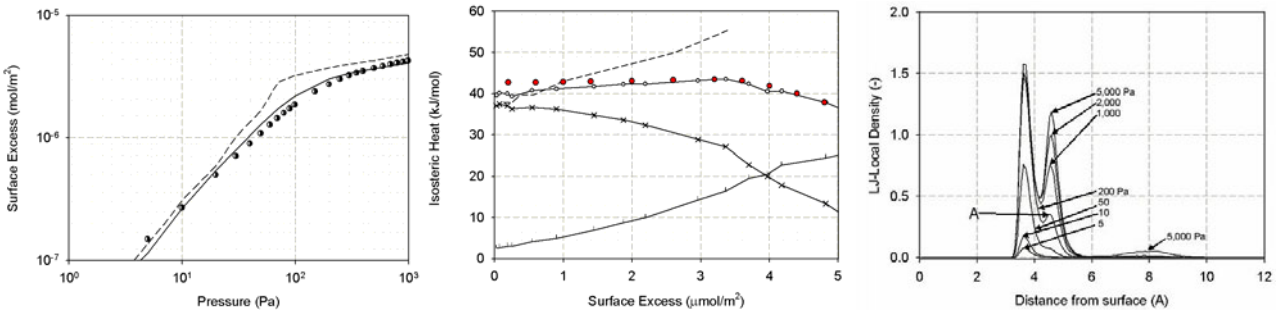

Figure 4: (a) Adsorption isotherm of benzene at 293 K (symbol: Data; solid line: simulation results with surface mediation; dashed line: simulation results with no surface mediation); **(b)** Isosteric heat versus loading (filled symbols: Data); **(c)** Local density distribution versus distance from the surface at 293K for P = 5, 10, 50, 200, 1000, 2000 and 5000 Pa

Interestingly when surface mediation is accounted for the isosteric heat is also well described by the adsorption model (Figure 4b), and the reasonably flat isosteric heat in the sub-monolayer region is due to the balance between the decrease of the solid-fluid contribution (solid line with cross symbols) and the increase in the fluid-fluid interaction (solid line with bar symbols). This effect is similar to what we have observed for carbon tetrachloride, i. e. the configuration of adsorbed molecules is changing with loading in this region. To test that the decrease in the solid-fluid contribution is due to a change in configuration of the benzene molecules, the local density distribution versus distance for a number of pressures is shown in Figure 4c. For low pressures (5 and 10 Pa), there is only a monolayer evident at a distance of 0.35 nm. This corresponds to

benzene particles aligning parallel to the surface. As the pressure increases, the first layer density increases but a new peak starts to develop at 0.45 nm (point A in Figure 4c). This is certainly not the second layer of benzene adsorption which occurs at a distance of about 0.8 nm. Rather it is a result of some of the benzene molecules adopting configurations between being parallel and perpendicular to the surface. As the pressure is increased, a higher fraction of molecules adsorbed are not parallel to the surface. Knowing the size of the benzene ring, benzene must have an angle of about 45^o to the surface, assuming some carbons still at a distance of 0.35 nm from the surface, for the centre of the ring to be 0.45 nm from the surface. So this causes the decrease in the solid-fluid contributions to the isosteric heat whilst the fluid-fluid contribution increases at the same time due to the greater contact between slanted benzene molecules compared to when they are parallel to the surface. The combined result is the constant isosteric heat versus loading in the sub-monolayer region.

4.4 Nitrogen

Let us now turn to nitrogen as this is the most widely used fluid in characterization by adsorption methods. There are a number of potential models for nitrogen, but the one by Murphy et al. (1980) is the one that we use because of its reasonable description of vapour-liquid equilibria (Do and Do, 2005f). There are two points arising from the simulation of adsorption. One is that the surface mediation needs to be accounted to correctly describe the approach to monolayer coverage, and the other is that the solid-fluid well-depth of interaction energy is slightly larger than the value calculated from the Lorentz-Berthelot rule. We argue that this is due to the interaction of nitrogen quadrupole with the surface, in addition to the dispersive interaction. This is accounted for in the molecular model by assuming that the surface contains some functional group and we take carbonyl as the representative group. Using the concentration of carbonyl as the fitting parameter to match the experimental Henry constant, we found that the concentration of carbonyl is 0.63 μmol/m^2. Given a carbon atom concentration on a graphene sheet as 63.4 μmol/m^2, this corresponds to 1% of the surface being covered with functional groups. This falls in the range that was reported in the literature. With the account for the surface mediation and the functional group, we obtain a fairly excellent description of isotherm and isosteric heat as shown in Figure 5.

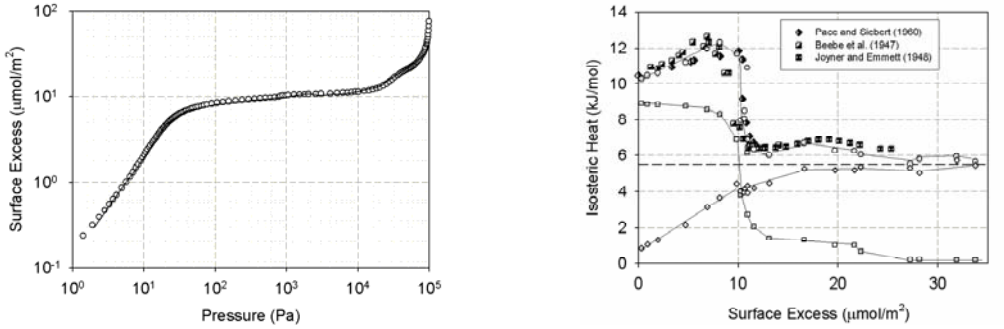

Figure 5: (a) Adsorption isotherm of nitrogen at 77 K; **(b)** isosteric heat versus loading

The small decline in the solid-fluid contribution to the isosteric heat (Figure 5b) is due to the fact that some nitrogen molecules take a vertical orientation when monolayer is approach. It is similar to what we have observed with carbon tetrachloride and benzene earlier. This is a common pattern that we have seen with fluids that have structure.

5. Adsorption of n-Alkanes

Before discussing the important group of polar fluids, we briefly discuss the adsorption of hydrocarbon and pay attention on the alkane family and see how the flexibility of long chain alkane in the adsorption on graphite surface. The transferable potential model of TRaPPE is used to model n-alkanes. This model accounts for not only the intermolecular dispersive interactions between two particles but also the intramolecular interactions, which arise from angle bending and torsion.

We consider C4 to C6, and investigate the flexible model of TraPPE against a model in which we assume no intramolecular interactions (Do and Do, 2005e). We have found that up to n-pentane the particle can be considered as rigid, but the difference between the two models begins to show with n-hexane. Thus it is concluded that for adsorption of n-alkane having carbon atom greater than 6 we have to use the flexible TraPPE model in preference to the rigid model.

6. Polar Molecules

We now finally consider what we regard as the most exciting group of fluids to deal with in adsorption, polar fluids. In the last section 4, we see that the influence of functional group might play an important part in the adsorption of nitrogen. But nitrogen is not a strong polar fluid. It only has a quadrupole, and therefore we would expect that the functional groups can play a very critical role in the adsorption of polar fluids. But first, what is so special about the polar fluids and why do they behave differently from simple fluids? Let us show this with the following figure (Figure 6a) where we compare the experimental isotherms of argon at 87.3 K and ammonia at 195 K (Birkett and Do, 2006a, b; 2007).

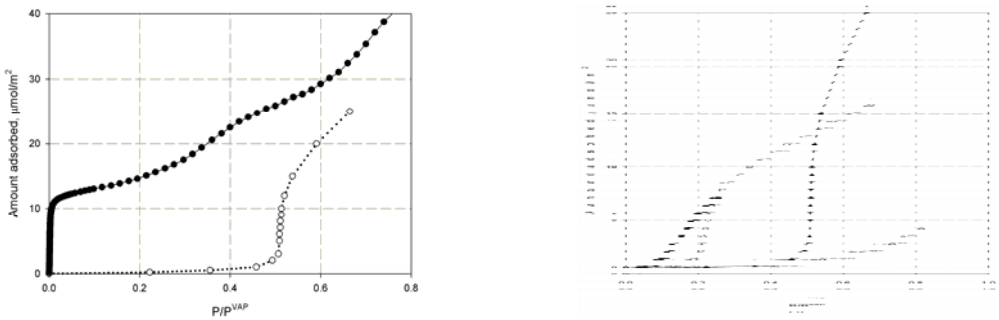

Figure 6: (a) Adsorption of argon at 87.3 K (solid symbols) and ammonia at 197 K (open symbols) **(b)** Exp. isotherms for ethanol at 307 K (●), methanol at 273 K (o), ammonia at 195 K (▲) and water at 302K (△).

The first distinct difference is the shape of the two isotherms, argon showing a Type II isotherm while ammonia exhibiting a Type III isotherm. This arises due to the interplay between the solid-fluid and fluid-fluid interactions. In the case of argon, the solid-fluid interaction dominates the fluid-fluid interaction in the region of sub-monolayer as seen in Figure 1c for loadings less than 10 μmol/m^2. It means that argon, when exposed to a graphite surface, adsorbs quite readily onto the surface. Only when a monolayer has been formed the dominance of the fluid-fluid interaction over the solid-fluid interaction is seen in the second and higher layers. On the other hand in the case of ammonia, the solid-fluid interaction is not sufficiently strong enough to induce the onset of adsorption at low pressures. Only when the pressure is high enough the onset of adsorption on the surface occurs, and when this is the case the strong fluid-fluid interaction (via hydrogen bonding) can induce the growth of so-called cluster around the molecules that previously have been adsorbed on the surface. This onset of adsorption is a critical factor in the adsorption of polar fluids, and the key parameter that affects this onset is the existence of strong sites that can induce (nucleate) the binding of the fluid molecule. These strong sites could be defects with the right size that can lock a molecule in place or functional groups with strong interaction energy towards the fluid particle. This will nucleate the adsorption of the first molecules, and these nucleating molecules can act as anchor for further adsorption of molecules around them. This is the growth of cluster phenomenon. Let us explore this a bit further by considering three polar fluids of varying degrees of fluid-fluid interaction, ethanol, methanol, ammonia and water. Among these, water has the highest fluid-fluid interaction and ethanol has the lowest, compared to solid-fluid interaction. Their isotherms on graphite are shown in Figure 6b for ethanol at 307K, methanol at 273 K, ammonia at 195K and water at 302 K. The increasing importance of fluid-fluid interaction over the solid-fluid interaction is clearly seen in the increasing dominance of Type III over the Type II. Ethanol has the ethyl group which interacts better with the surface, and it has to compete with the hydrogen bonding between the oxygen of one molecule and the hydrogen (of OH) of another molecule. Moving to methanol in which the hydrocarbon part (methyl group) becomes shorter and therefore the dispersive interaction with the surface is weaker, we see the dominance of the fluid-fluid interaction via bonding over the methyl group interaction with the graphite surface.

The nucleation depends not only on the concentration of the functional group but also the topology of the functional groups. If the groups are widely separated (i.e. no cooperation between them), the rate of nucleation is directly proportional to the concentration of the functional group. However, if they are close together, the effect can be more than the combination when they are separated and it also can be less than that. This depends on the configuration of the close-by functional groups. We study this with a number of model surfaces that are loaded with functional groups. These models are shown in Figure 7. The first model is a bare surface (not shown). The others are 5 carbonyls, 9 even spaced carbonyls, 9 evenly spaced groups of 5 carbonyls and 49 evenly spaced carbonyls.

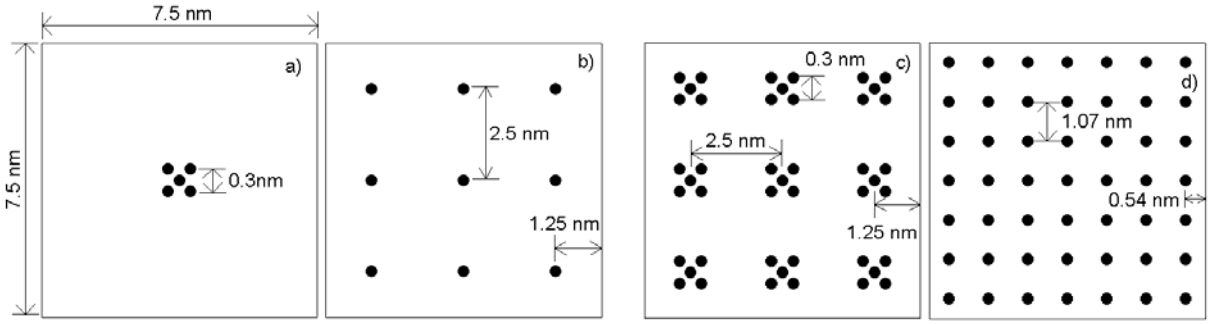

Figure 7. Configurations of carbonyls (represented as filled circles) on the bottom plane of the pore a) group of five carbonyls located at the centre of the pore wall, b) nine evenly spaced carbonyls, c) nine evenly spaced groups of five carbonyls and d) 49 evenly spaced carbonyls. All configurations have the same box length of 7.5 nm.

6.1 Ethanol and Methanol

These configurations of functional groups were used in the GCMC simulation, and the simulated isotherms are shown in Figures 8a and 8b for ethanol and methanol, respectively. These simulation results agree qualitatively with the experimental isotherms shown in Figure 6b. Common in Figures 8a and b for ethanol and methanol is that the increase in the concentration of functional group results in an increase in the amount adsorbed. This can shift the Type III to Type II isotherm if the functional group concentration is high enough.

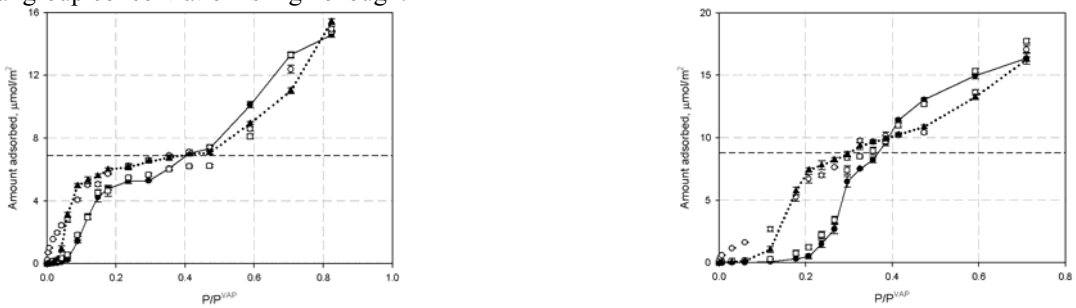

Figure 8: (a) Simulation isotherms for ethanol at 300 K on a carbon surface with: no carbonyls (filled circles with solid line), 5 carbonyls separated by δ = 0.3 nm (empty squares), 49 evenly spaced carbonyls (filled triangles with dotted line) and 9 evenly spaced groups of 5 carbonyls with δ = 0.3 nm (empty circles). Horizontal dotted line indicates monolayer coverage.
(b) Simulation isotherms for methanol at 300 K on a carbon surface. Symbols as in (a)

The 49 evenly spread carbonyls makes a larger difference to the adsorption by significantly decreasing the uptake pressure, and the 9 groups of five carbonyls (45 carbonyls in total) cause the largest increase in adsorption with initial adsorption more like type II isotherm behaviour. So it is not just simply the concentration of the functional groups but also its configuration which strongly affects the adsorption behaviour.

The simulation results on the bare graphite surface at 300 K are compared against the experimental results as shown in Figures 9a and b for methanol and ethanol, respectively. These figures show a reasonably good agreement between the simulation results and the data. This will also be true for the case where the surface only has a small number of carbonyls on the surface, such as the isotherms for the single group of five carbonyls. So it is not possible to differentiate between a surface with a small number of functional groups and that without using the experimental isotherms. One thing, however, is clear that simulated isotherms with large number of functional groups can not describe the data, and we can rule out the high concentration of functional groups on graphitized thermal carbon black. Although we mentioned earlier that the presence of function group is to induce the nucleation, so why are the simulated isotherms for a bare surface and a surface with low concentration of functional group almost the same for this case of ethanol and methanol? This is due to two reasons. First the anchoring effect is done with ethyl group and methyl group, and the affinity of carbonyl group toward ethanol and methanol is not strong enough to overwhelm the anchoring effect of ethyl and methyl groups.

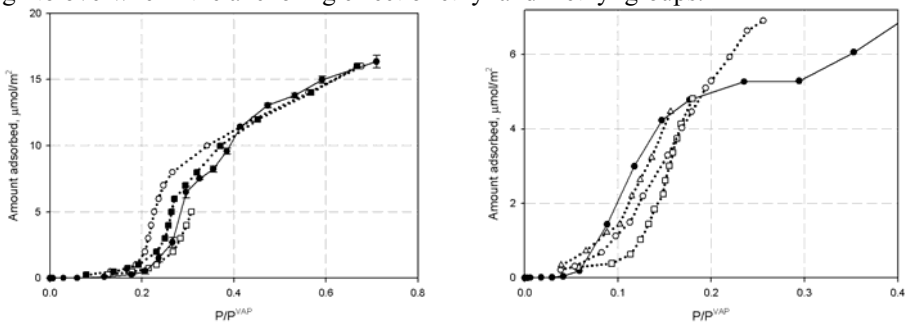

Figure 9: (a) Experimental adsorption isotherms for methanol on carbon black at various temperatures: 273.15 K (empty circles with dotted line), 293.15 K (filled squares with dotted line) and 326.15 K (empty squares with dotted line). Simulation results at 300 K (filled circles with solid line) for a surface with no carbonyls.
(b) Experimental adsorption isotherms for ethanol on carbon black at various temperatures: 278.15 K (empty squares with dotted line), 293.15 K (empty triangles with dotted line) and 307.15 K (empty circles with dotted line). Simulation results at 300 K (filled circles with solid line) for a surface with no carbonyls.

We have seen that the adsorption isotherm on a bare surface and that on a surface with low functional group are practically close to each other. So how could we discriminate between these? The answer lies in the isosteric heat versus loading as the heat released per unit incremental of adsorption depends on the strength of interaction at the given loading. Figure 10a shows the isosteric heat versus loading for ethanol and methanol for the case of bare surface and a surface with a group of five carbonyls. The range of loading covered in this figure is inside the monolayer region. The monolayer concentration of ethanol and methanol are 6.65 and 8.8 μmol/m^2, respectively. It is clear in the investigation of the isosteric

heat that the distinction between the bare surface and the surface with low functional group concentration is imminent. The bare surface has heat at zero loading that is lower than the condensation heat, and this is because the solid-fluid interaction is less than fluid-fluid interaction of the bulk phase. The surface with low concentration of functional group has the zero-loading heat that is greater than condensation heat, and this is due to the stronger interaction between a fluid particle and the functional group than the fluid-fluid interaction in the bulk liquid phase. Over the sub-monolayer coverage region, the bare surface has a pattern of increasing heat with loading while the other surface has a decreasing heat with loading. At a loading of about 0.5 μmol/m^2, about less than 10% of the monolayer coverage concentration, these two curves practically coincide, suggesting that the mechanism of adsorption after this point is the same for both surfaces. This means that once there is an anchor on the surface the adsorption of methanol or ethanol is due to hydrogen bonding with the anchored particles aided by the dispersive interaction with the graphene surface. This is the growth of cluster, but how does this growth spread? Is it a cluster growth along the surface or is it a growth in all directions. But before we explore this we consider how various interactions (fluid-fluid, fluid-solid, fluid-functional group) contribute to the isosteric heat of adsorption.

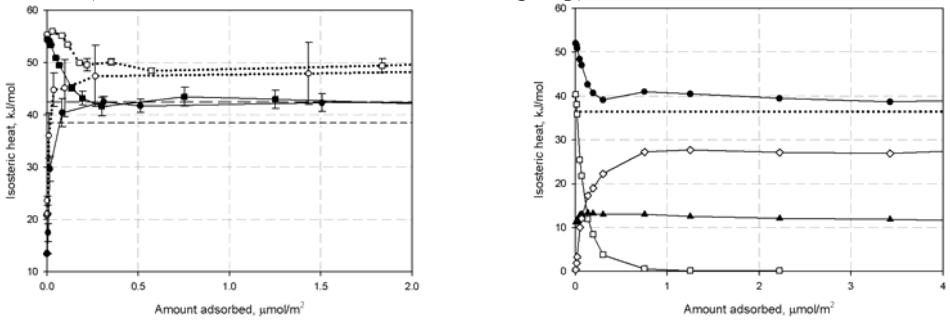

Figure 10: (a) Heats of adsorption from simulations for methanol (filled symbols) and ethanol (empty symbols) with a surface having no carbonyls (o, •) and a surface with a 5 centre configured carbonyls (□, ■). Horizontal short and long dashed lines indicate the heats of vaporization of the methanol and ethanol, respectively.
(b) Heats of adsorption for methanol on a surface with a single group of 5 carbonyls separated into its contribution from: fluid-carbonyl interactions (□), fluid-surface interactions (▲), fluid-fluid interactions (◊) and the total configurational contribution to the isosteric heat (•). Horizontal dotted line indicates the heat of vaporization.

Figure 10b shows these contributions that make up the isosteric heat for the case of methanol adsorption on a surface with a group of five carbonyls. As seen in this figure, the heat is initially dominated by the contribution from the fluid-functional group interactions. As loading increases this quickly decays to zero suggesting that a single group of carbonyls is quickly saturated and play no further part in adsorption. The solid-fluid contribution is practically constant, suggesting that methanol adsorption in the sub-monolayer region is a two-dimensional clustering. The fluid-fluid contribution to heat increases with loading up to about 1 μmol/m^2 (which is about 10% of the monolayer concentration), beyond which it remains constant. The constancy of the fluid-fluid contribution is due to the growth of cluster at the periphery, and as such each new methanol molecule adsorbing onto the surface will see the same number of neighbours. These behaviours that we just discussed for methanol apply to ethanol as well. The only difference is the solid-fluid interaction of ethanol is greater than that of methanol by 7 kJ/mol, and this is simply due to the additional carbon group.

Thus we have shown the nucleation and the growth of cluster in two dimensions. This is indeed confirmed with a snap shot of methanol and ethanol in Figures 11a, b for adsorption on a bare surface at 300 K. These snap shots show the formation of group of four or higher numbers of molecules, and such a formation is to maximize the hydrogen bonding formation. This is supported by the radial distributions of O-O and O-H as shown in Figure 11c. The first peak corresponds to hydrogen bonding while the second to the dimension of the square structure.

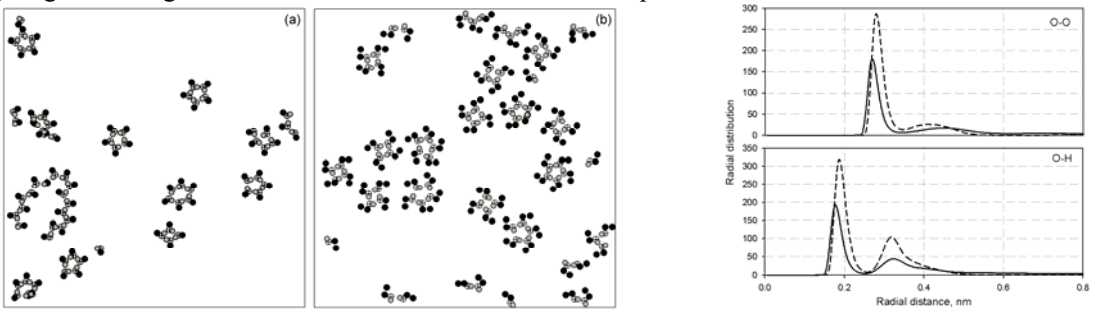

Figure 11. (a) Snapshot of methanol at a reduced pressure of 0.27. CH_3 (black), O (cross) and H (gray).
(b) Snapshot of ethanol at a reduced pressure of 0.09. CH_3 and CH_2 (black), O (cross) and H (gray).
(c) Oxygen-oxygen (O-O) and oxygen-hydrogen (O-H) radial distributions for methanol (solids lines) and ethanol (dashed lines) at 4.5 and 0.75 kPa, respectively.

6.2 Ammonia

We now turn to ammonia and this fluid has stronger fluid-fluid interaction than solid-fluid interaction, compared to ethanol and methanol that we just dealt with. The distinction between ammonia and alcohols is the sharp change in the amount adsorbed at a reduced pressure of 0.5 as seen in Fig.12a for ammonia adsorption at 240K. Adding more functional groups slowly shifts Type III isotherm closer to Type II because of the strong affinity of functional group toward ammonia.

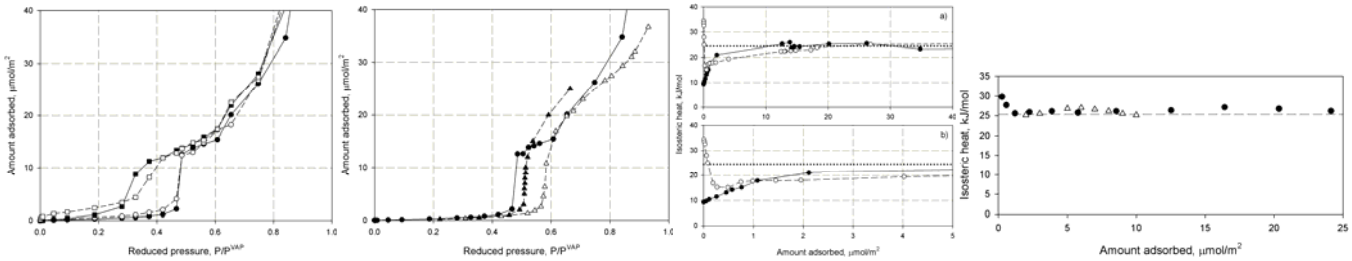

Figure 12. (a) Simulation isotherms for ammonia at 240 K on a carbon surface with: no carbonyls (•), 5 carbonyls separated by δ = 0.3 nm (o), 49 evenly spaced carbonyls (■) and 9 evenly spaced groups of 5 carbonyls with δ = 0.3 nm (□).

(b) Experimental isotherms for ammonia at 194K (△) and 195.15K (▲) with the simulated isotherm 240K (•).

(c) Isosteric heats of adsorption for ammonia on carbon black from simulation for a surface with no carbonyls (•) and a surface with a single group of 5 carbonyls (o). The horizontal dotted lined corresponds to the enthalpy of vaporisation

(d) Experimental heats for ammonia on highly graphitized carbon black. Horizontal line is the vaporization heat

Experimental data of ammonia adsorption on GTCB are shown in Figure 12b together with the simulation results on a bare surface. The simulation results basically capture the pattern of adsorption isotherm. Even the simulation results on a surface with low functional group concentration also capture the same pattern. This feature is exactly the same as that we have observed earlier with alcohol. The distinction between these two surfaces can only be made with the consideration of isosteric heat versus loading as shown in Figure 12c. Like alcohols, the heat at zero loading for the case of bare surface is below the condensation heat, and the isosteric heat increases with loading. In the case of a surface with a group of five carbonyls the zero-loading heat is higher than the condensation heat (which is due to the greater affinity of ammonia with the functional groups). The heat then decreases with loading to a local minimum and then increases to the condensation heat. At loadings greater than 0.5 μmol/m^2 the heat curves for these two surfaces are practically the same, suggesting a similar adsorption mechanism for both surfaces. Thus we see that the adsorption behaviour of ammonia is similar to what we have seen with alcohols, with the exception of minimum in the heat curve observed with ammonia adsorption on a surface with a group of five carbonyls. This behaviour is in agreement with the experimental data as shown in Figure 12d, suggesting that the GTCB has a low concentration of functional group. Let us now explore the isosteric heat further by decomposing it into various contributions, and this is shown in Figure 13. From this, we see that the fluid-functional contributions are the dominant contribution at low loading, suggesting a nucleation mechanism that we have discussed with alcohols. As the loading increases, this contribution decreases rapidly, meaning that the carbonyl group is saturated with ammonia and has no further part in adsorption. The solid-fluid contributions are almost constant indicating that adsorption occurs in the monolayer only with no three dimensional structures forming. The fluid-fluid contribution increases with pressure and becomes greater than the solid-fluid contribution well below monolayer coverage. This is in contrast to the case of argon where the solid-fluid contribution only fall below the fluid-fluid contributions as the monolayer is being completed and the second layer started. The reason why the isosteric heat has a local minimum is that the fluid-functional group contribution decays very rapidly, suggesting the quick saturation of the functional group with ammonia molecules.

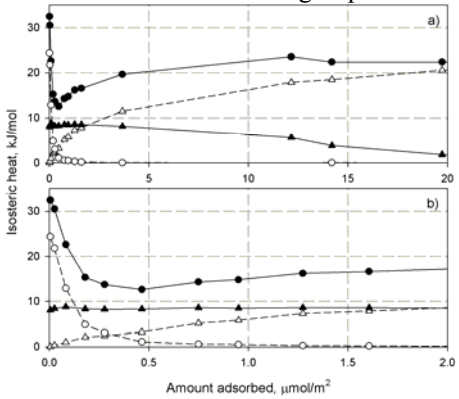

Figure 13. Simulation isosteric heats for a surface with a single group of 5 carbonyls split into its contributions: total configurational isosteric heat l (•), fluid-fluid (△), fluid-solid (▲) and fluid-functional (O).

6.3 Water

Water is perhaps the most interesting species to deal, and this is almost attributed to its unique very strong hydrogen bonding. This is reflected in the fact that practically no adsorption of water on a bare surface is observed in simulation (Birkett and Do, 2007). Therefore to study water adsorption in a meaningful way, we have to consider functional group and the selection of functional group is also important because we have to ask a question that which functional group is adequate to have sufficient interaction with water molecule and to have reasonable competition with the fluid-fluid interaction. There are, of course, many ways that we could choose the functional group type, concentration and topology. The role of the functional group is to provide anchoring role for water to nucleate and then grow in cluster size. To mimic this role, we artificially fix one or more water molecules on the surface and study the nucleation and clustering. With a water molecule fixed on the surface, Figure 14a shows a snap shot of water adsorption and we see the basic structure of cluster is a pentamer. Without this anchor, the chance of this type of structure spontaneously forming on a bare surface is extremely small. The notion of basic structure suggests that water when adsorbed onto the surface will take the form of basic structures. This can be investigated by studying the number histogram plot, which is essentially the fraction of configurations during the course of a simulation. This is shown in Figure 14b for the case of a graphite surface with one water molecule fixed on the surface. The distinct feature that we note from this plot is that the distribution is not smooth, but rather we observe peaks at some definite numbers, meaning that water tends to form as groups on the surface. This is to favour the hydrogen bonding. The dominant configuration for two of the pressures, 0.6 and 0.7 kPa, is to have zero water molecules in the simulation. Clearly the next most preferred configuration is with either three or four molecules in the system. This corresponds to the tetramer and pentamer like structures that we just discussed. The next thing to notice is that there is a large range of configurations that contribute to the ensemble average number of molecules. For the case of 0.8 kPa where the ensemble average of molecules was only 5.4 but configurations with up to 25 molecules contributed significantly to this average. So the clusters about the fixed water molecule continuously grow and evaporate again during the course of the simulation.

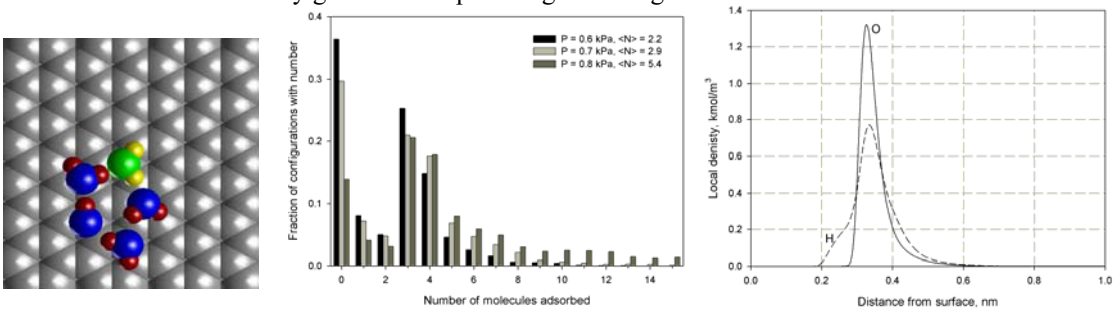

Figure 14. (a) Snapshot of water (blue and red) on graphite with a single fixed water molecules (green and yellow). **(b).** Histogram of number of particles adsorbed in the simulation for a surface with a single fixed water molecule. **(c).** Density as a function of distance from carbon surface for the case of a surface with a single fixed water molecule, SPCE water and P = 0.7kPa. Solid and dashed lines denote oxygen and hydrogen density, respectively.

To further confirm the two dimensional cluster, we consider the z-distributions for the water. Figure 14c shows the z-distributions for the oxygen and hydrogen atoms of the water molecules at 0.7 kPa on a surface with one fixed water molecule. This shows that the adsorption of water is completely in the monolayer with no indication of any three dimensional clustering. The alignment of the hydrogen peak with the oxygen peak shows that flat two dimensional clustering is the dominant configuration for water.

To compare the adsorption that one gets from the fixed water and carboxyl groups, the results of simulation using these two functional groups are presented in Figure 15. The adsorption for this surface with fixed water molecules is closer to the experimental isotherm than for the other cases considered but is still well short. This means that real surfaces must exhibit greater attraction toward water, and this is the subject of great interest and is being investigated.

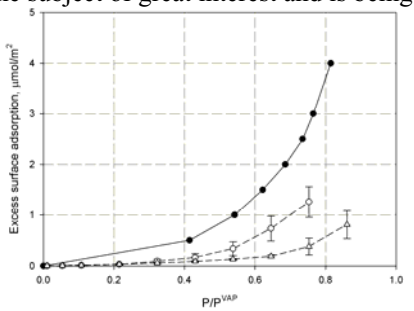

Figure 15. Adsorption on graphitised thermal carbon black from experiment (filled circles) with simulation results for a surface with 4 groups of 2 fixed waters (empty circles) and 4 groups of 2 carboxyls (empty triangles).

7. Supercritical Adsorption

The discussion of adsorption of simple and complex fluids is restricted to that at sub-critical conditions. Adsorption at temperatures above the critical point has been a subject of great interest in recent years, and this comes about because of the interest in storage of high energy gases in porous media. With the molecular simulation tools, we are beginning to shed more light into the way how fluids in the adsorbed phase behave under supercritical conditions. In molecular simulation, we define excess amount for adsorption on a surface as the surface excess Γ_{excess}, while for the case of slit pore, it is in terms of excess pore density ρ_{excess}. They are, respectively, obtained from the GCMC simulation as below:

$$\Gamma_{excess} = \frac{\langle N \rangle - (H - z_0) L_x L_y \rho}{L_x L_y}; \qquad \rho_{excess} = \frac{\langle N \rangle}{L_x L_y (H - 2z_0)} - \rho$$

where z_0 is the distance (from the plane passing through the outermost layer of carbon atoms) at which the solid-fluid potential is zero, σ_{ff} is the collision diameter of adsorbate molecule, <N> is the ensemble average of the number of particle in the simulation box, ρ is the bulk gas density, and L_x and L_y are the simulation box lengths in the x- and y-directions, respectively. The void volume used in the GCMC simulation is the volume accessible to particle center at zero loading.

7.1 GCMC simulation of GTCB

Figure 16a shows the isotherm of surface excess in terms of pressure (top curve) and the bulk gas density versus pressure in the bottom curve for the case of argon adsorption on GTCB at 253 K. There are a number of distinct features that we could derive from this super-critical adsorption isotherm for an open surface (Do and Do, 2005g).

1. The excess density exhibits a maximum.
2. The decreasing portion of the surface excess isotherm is more gradual than the increasing part, and this gradual decrease is in phase with an increase of the bulk density.
3. Up to 100 MPa (~1000 atm), the surface excess remains positive

If we now present the isotherm as the plot of the surface excess density versus the bulk gas density as shown in Figure 16b in log-log scale, more features emerge. In the low pressure region, we observe Henry law behaviour as reflected in the slope of unity (dashed line). On the other hand, in the region of high pressure, we see the curve also approaches a linear asymptote. This means that the surface excess has the following asymptote with density as $\sim \rho^{-n}$ ($n > 15$). Thus the difference between the average density of the adsorbed layer and the bulk gas density decays as $1/\rho^n$. This also means that the average density of the adsorbed layer never reaches a constant as assumed in many work, but rather it increases in excess of the bulk density by an amount given in the above equation, at least over the pressure range studied in this work.

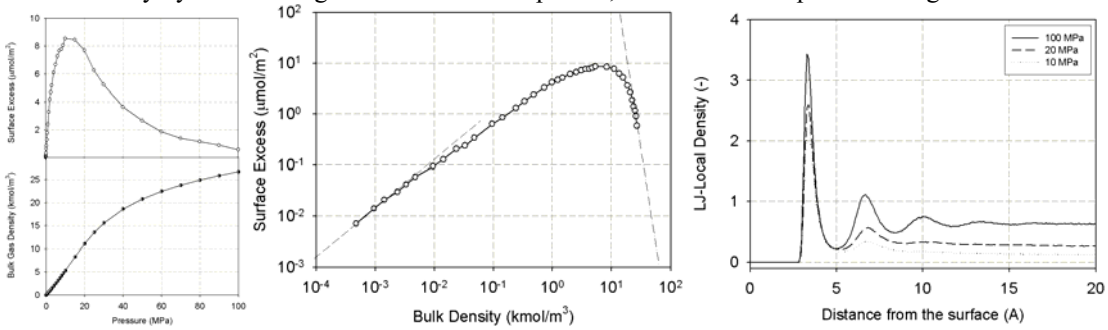

Figure 16: **(a)** Surface excess (top) and bulk gas density (bottom) versus pressure for argon adsorption on graphite at 253 K; **(b)** Surface excess versus bulk gas density; **(c)** 2D-density distribution of argon versus distance from the surface at three values of pressure (10, 20 and 100 MPa)

To understand how adsorption occurs on the surface as a function of pressure, we present in Figure 16c the local density distribution versus distance from the surface at 253 K. This figure shows that the adsorption has a layering mechanism with layers being parallel to the flat surface of graphite. This is similar to that observed with adsorption under sub-critical conditions. We see that at the highest pressure studied, 100 MPa (1000 atm), there are three layers that can be identified on the surface with the singlet density of the first layer being substantially greater than that of the other layers. Another point that we observe is that the density of the first layer is constantly increasing (even up to a pressure of 100 MPa) but with a reduced rate at very high pressures. The three distributions shown in Figure 16c for three values of pressure, 10, 20 and 100 MPa show that the densification of the first layer which has a propagating effect on the densification of the second layer. The propagation effect extends to the third layer at very high pressures. Note that the pressure 10 MPa is the pressure at which the surface excess is maximum while the pressure 20 MPa is the pressure at which the fluid-fluid interaction starts to dominate the solid-fluid interaction. To further illustrate the densification (rather than condensation) of argon under

supercritical condition, we present in Figure 17 the snap shots of particles of the first layer for the same three values of pressure used in the plots of local density distribution in Figure 16c (P = 10, 20 and 100 MPa).

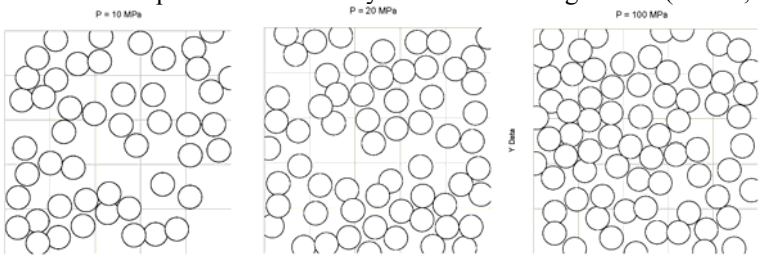

Figure 17: Snap shots of argon particles in the first layer at 253 K for (a) 10 MPa; (b) 20 MPa; (c) 100 MPa

We can see from these snap shots that there are still vacant spaces in the first layer even at very high pressures (100 MPa ≈ 1000 atm in Figure 17c). Particles tend to form clusters and as pressure increases the clusters either increase in size or agglomerate to form larger clusters. This is called the densification, and it is the characteristics of super-critical fluid, that is no condensation in either two dimensions or three dimensions.

7.2 Graphitic Perfect Slit Pores

Investigation of adsorption of slit pores requires an understanding on the effect of width on adsorption. Beside the enhancement on the adsorption potential the pore width can influence adsorption in a way that the pore can pack an integral number of layers. Those pores that can pack exactly an integral number of layers under moderate conditions are called the perfect pores, and other pores are designated imperfect pores. Let us start with the first perfect pore of 6.5 A.

6.5 A (One-layer pore)

This pore can accommodate neatly one integral layer, and since the enhancement in the solid-fluid potential in this pore is significant the adsorption occurs at a pressure lower than those of larger pores. Figure 18a shows the excess pore density (curve with circle symbols) in terms of the logarithm of pressure, while Figure 18b presents the same plot in linear scale. We see that the maximum of the excess pore density versus P (at 5 MPa) is very clear, like what we have observed with an open surface earlier in Section 7.1 but the pressure at which the maximum occurs (p_m) for the case of an open surface is 12.5 MPa. Thus the pressure p_m shifts to lower values for smaller pores.

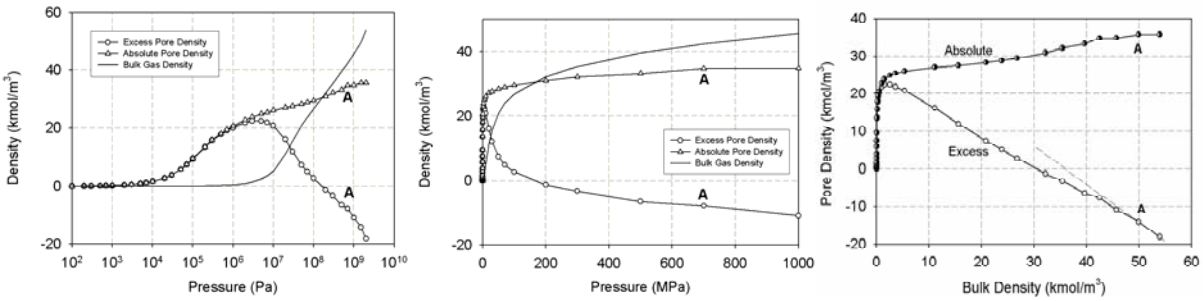

Figure 18: Plot of the excess density (circle symbols), absolute pore density (triangle symbols) and bulk gas density (solid line) **(a)** log-scale of pressure axis; **(b)** linear scale of pressure axis; **(c)** Plot of the excess and absolute pore density versus bulk gas density for slit pore of 6.5 A and at 253 K

Another two features observed with slit pores are not manifested with adsorption on open surfaces. One is the negative excess pore density and this is simply because it is easier to compact particles in the three-dimensional space of the bulk phase than to do so in two-dimensional space at extremely high pressure, resulted from the greater fluid-fluid interaction than the solid-fluid interaction. This transition from the positive excess pore density to the negative one occurs at an extremely high pressure of 200 MPa (~ 2,000 atm!), at which the pore density is becoming less than the bulk gas density. Another feature noted is the small shoulder on the decaying part of the isotherm, which occurs at about 700 MPa (point A in Figure 18). To find out the reason for this small shoulder, we plot the absolute pore density as well as the bulk gas phase density as a function of pressure, as shown in Figure 18b as the line with triangle symbols and the solid line, respectively. It is clear that the small shoulder is due to the fact that the maximum packing in the pore has been reached while the bulk density keeps increasing. We have $n_{excess} = n_{abs} - V\rho_b$. Following this equation the shoulder is resulted from the absolute pore density achieving its saturation value of 34 kmol/m^3. From point A onwards (pressures higher than the pressure at A, 700 MPa), we have constant absolute pore density while the bulk gas density is steadily increasing, leading to the linear decline of the excess pore density with respect to the bulk gas density as shown in Figure 18c where we plot the excess pore density versus the bulk gas density. In this figure, not only we see the linear behavior for pressure greater than 700 MPa (corresponding to

the bulk density greater than about 50 kmol/m^3), we also observe a linear behavior in the range of bulk gas density from 5 to about 25 kmol/m^3. The linear behavior in this range is not due to the constancy of the density but rather to its approximate linear increase in this range.

It is worthwhile at this point to show the difference between the supercritical adsorption and sub-critical adsorption in this 6.5 A slit pore. We choose 87.3 K as the temperature for sub-critical adsorption, and 253 K for supercritical adsorption. The pore densities versus pressure for these two conditions are plotted in Figure 19. The vapor pressure of 87.3 K sub-critical adsorption is 1.013×10^5 Pa. It is clear that adsorption under sub-critical conditions occurs at much lower pressures than the supercritical conditions. The absolute (circle symbols) and excess pore densities (solid line) for the sub-critical conditions are practically superimposed on each other, and this is simply due to the much lower bulk gas density compared to the pore density. On the other hand, in the case of supercritical conditions these two densities agree with each other at low pressures (P < 1 MPa) but deviate from each other when the maximum is observed. As mentioned earlier this is due to the combined sharp change in the bulk density versus pressure and the slower rate of increase in the absolute pore density.

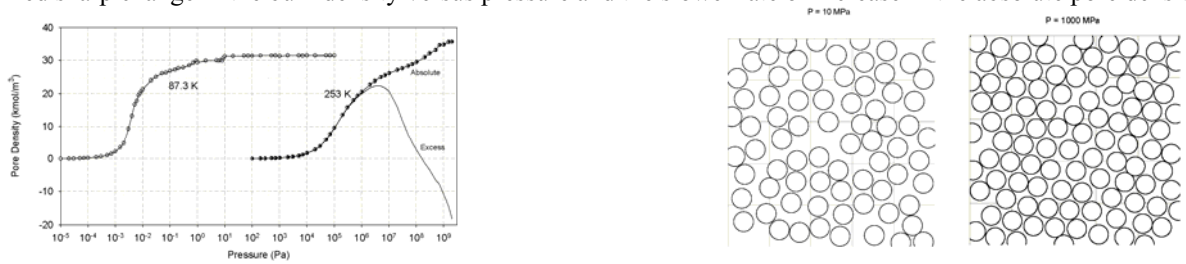

Figure 19: (a) Comparison between sub-critical adsorption at 87.3 K and supercritical adsorption at 253 K **(b)** Snap shots of argon in 6.5 A slit pore at 253 K (P = 1, 10, 1000 MPa)

To show the degree of compression of two-dimensional fluid in this 6.5 A pore, we plot in Figure 19b the snap shots of particles for two values of pressure, 10 and 1000 MPa. It is clear in these figures that at 10 MPa, the packing is still far from perfect, and it is not until extremely high pressures greater than 700 MPa (~7,000 atm!) that we will see a nearly perfect hexagonal packing. This pressure corresponds to the point A in Figure 18. This packing can not be further compressed with a further increase in pressure as reflected in the constancy of the absolute pore density.

7.3 Graphitic Imperfect Slit Pores:

Here we shall choose two imperfect pores to illustrate the differences between perfect pores and imperfect ones. They are 8 A and 11.5 A pores. Under normal conditions of moderate pressures, the 8A pore is too large for one layer and too small for two layers, while the other pore, 11.5 A, is too large for two layers and too small for three layers.

Let us consider the excess pore density of these two so-called imperfect pores. The plots versus pressure are shown in Figures 20. Yet again we observe the maximum phenomenon, but we also note a number of distinct differences from what we have observed before with perfect pores.

1. The pressure at which the excess pore density becomes negative is much lower than that for perfect pores
2. The absolute pore density seems to reach a plateau of low density because of the imperfect packing. Only when the pressure is very high that the absolute pore density increases from that apparent low plateau of density to the final saturation level. This increase occurs in a number of stages
3. Between the two imperfect 8 and 11.5 A pores, it is easier to pack argon particles in the 11.5 A pore because of the larger volume space for rearranging the particles.

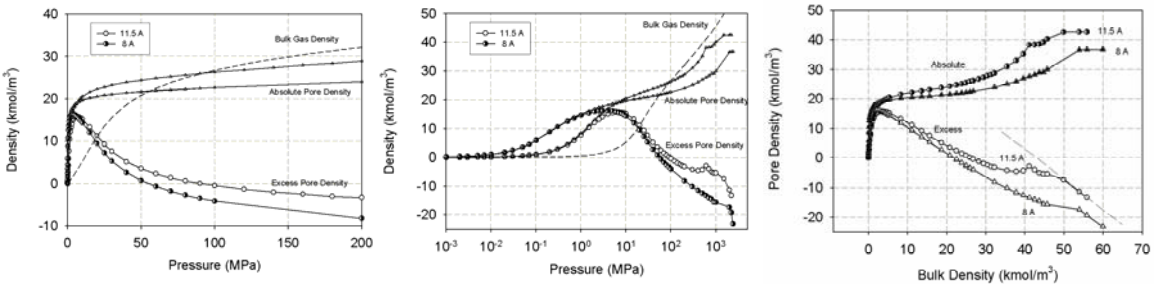

Figure 20: Plot of excess pore density (circle symbols), absolute pore density (triangle symbols) and bulk gas density (dashed line) versus pressure for 8 and 11.5 A pores (Left figure: linear pressure scale; Right figure: logarithm pressure scale); (c) Plot of absolute and excess pore densities versus bulk gas density for 8 and 11.5 A pore at 253 K.

Let us explain these points. The reason for the excess pore density to become negative sooner is because the absolute pore density attains an apparent plateau of low density, which is a direct result of the imperfect packing. It is only when the pressure is increased much further, the chemical potential is great enough to overcome the repulsion between particles. This

allows the particles to be compressed to form two distinct layers in the case of 8 A pore and three distinct layers in the case of 11.5 A pore. This is clearly supported by the 2D-density distribution of argon in those pores, as seen in Figure 21. At low pressures, the chemical potential is not great enough and particles can not form two distinct layers in 8A pore. This is shown as two substantially overlapped peaks in Figure 21a. However, when the pressure is very high, we see the overlapped peaks split into two distinct peaks for the case of 8A pore and into three peaks for the case of 11.5A pore. As a result of this splitting, the absolute pore density increased very sharply as seen in Figures 20.

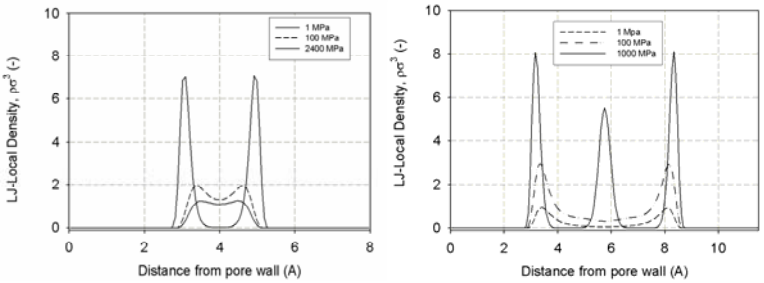

Figure 21: Local density distribution versus distance from pore wall (Left figure: 8 A pore; Right figure: 11.5 A pore).

8. Non-Graphitized Carbon Black

Up to this point, we have dealt with graphite surface or graphitized thermal carbon black (GTCB), which is highly homogeneous. Now we consider non-graphitized carbon black (NGCB), and we shall model it as a collection of graphene layers with the top layers being defective. To model a surface with defect, we select in random a carbon atom in this surface and remove it as well as all surrounding neighbours whose distances to the selected atom less than an effective defect radius, R_c. We repeat this random selection until the percentage of carbon atoms removed has reached a given value. Thus the two important parameters for modelling of a non-graphitized surface are the percentage of defect and the size of the defect, which is measured by the effective radius R_c.

8.1 Comparison between adsorption of argon on GTCB and that on NGCB

The difference between the adsorption on GTCB and NGCB can be shown in Figure 22a, where we plot the data of argon on GTCB at 87.3 K taken from Olivier (1995) and those on NGCB taken from Gardner *et al*. (2001) for BP 280 (a non-graphitized carbon black) as the dashed and solid lines, respectively.

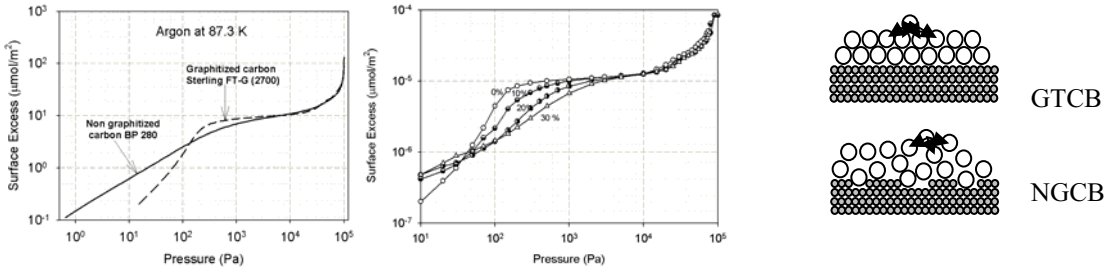

Figure 22 (a) Experimental adsorption isotherms of argon at 87.3 K on GTCB and NGCB
(b) Simulated adsorption isotherms of argon at 87.3 K on NGCBs with defect percentage varying from 0 to 30 %
(c) Schematic diagram of molecular interaction at higher layers for NGCB and GTCB

The differences between these two experimental data are given below.

1. The NGCB has a greater adsorbed density at low pressure, and this is due to the effects of surface heterogeneity for which argon adsorbs initially onto strongest sites of BP280.
2. Once the first layer has been completed, the surface heterogeneity does not affect adsorption in second layer
3. Adsorption on BP280 shows smooth behavior with no well defined plateau of monolayer, while that on GTCB shows a distinct monolayer. This is due to the irregular packing in the case of NGCB, compared to ordered fashion exhibited in GTCB. This is shown in Figure 22c.
4. At low loadings, the adsorption isotherm of GTCB shows a slope of unity in the log-log plot, indicating the Henry law behavior. However, in the case of NGCB, Henry law is never observed, this is due to the initial adsorption of particles onto the strongest sites and the further adsorption on progressively weaker sites. This progressing leads to a decrease in the adsorption affinity that Henry law cannot be observed for NGCB. Strictly speaking, Henry law should also be observed for NGCB, but this occurs at extremely low pressures (lower than practically measured pressures) where adsorption is that of molecules residing in the strongest sites on the surface.

This difference between GTCB and NGCB can be described by the molecular models of a perfect surface and a defected surface. Figure 22b shows the adsorption isotherm of GTCB and those of defected surfaces with various defect percentages (Do and Do, 2006c), and we see that these simulation results capture correctly the experimental adsorption isotherm.

8.2 Comparison with experimental data of Beebe and Young (1954)

Experimental data for adsorption on surfaces with various degrees of graphitization are scarce in the literature. The few data are those of argon adsorption on surfaces with different degrees of graphitization from Beebe and Young (1954). The non-porous carbon black used by them is Spheron 6. This sample was subject to heat treatment for two hours at various temperatures to produce Spheron (1000), Spheron (1500), Spheron (2000) and Spheron (2700). The number in the bracket is the treatment temperature.

Figure 23 shows the experimental isosteric heat data of argon (circle symbols) at 77K on surfaces of varying degrees of graphitization. The heat curve for Spheron (1000) indicates the dominance of the surface heterogeneity over the fluid-fluid interaction, while that of Spheron (2700) indicates the opposite. Using the GCMC simulation results for argon adsorption at 77 K on surfaces of various degrees of defect, we have found that the simulation results for the surfaces with 20, 10, 5 and 0% defect and the effective defect radius of 2.84 A yield the heat curves that are in good agreement with Spheron samples treated thermally at 1000, 1500, 2000 and 2700 C, respectively. This means that Spheron (2700) behaves very much like a homogeneous graphite surface, which is well known in the literature. The agreement of the isosteric heat versus loading for argon adsorption on surfaces of different degrees of graphitization suggests that the model proposed in this paper is a potential one for wider applications, such as modelling of adsorption in activated carbon. The isosteric heat curve versus loading for Spheron 6 (untreated) indicates that it is a very heterogeneous surface (circle symbols in Figure 23a) because the isosteric heat decreases continuously versus loading. Because it is very heterogeneous, we simulate the surface with very high extent of defect (50%) and larger effective defect radius of 4.23 A (compared to 2.84A in the cases of heat-treated samples) and find that the isosteric heat curve has a similar pattern as that observed experimentally.

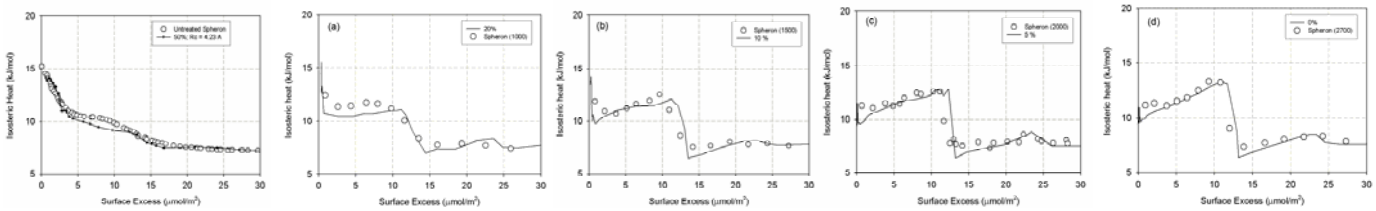

Figure 23: Comparison between experimental isosteric heat data and GCMC simulation of adsorption of argon on surfaces of NGCB. (a) Spheron (1000); (b) Spheron (1500); (c) Spheron (2000); (d) Spheron (2700); (e) untreated Spheron.

8.3 Analysis of adsorption of argon and nitrogen on BP280

Using the molecular model with surface defect, we simulate the experimental data of argon on BP280 at 87.3 K, and we have found that the model with surface having 29% defects and a defective radius of 4.92 A can describe well the data (Figure 24a). Are these parameters purely adjusting parameters or do they bear some physical significance? If they are to have some physical meaning, they must be independent of the adsorption temperature and the choice of molecular probe. To test this we consider the adsorption data of argon on the same sample, BP280, at a lower temperature, 77K, and the adsorption data of nitrogen at 77 K.

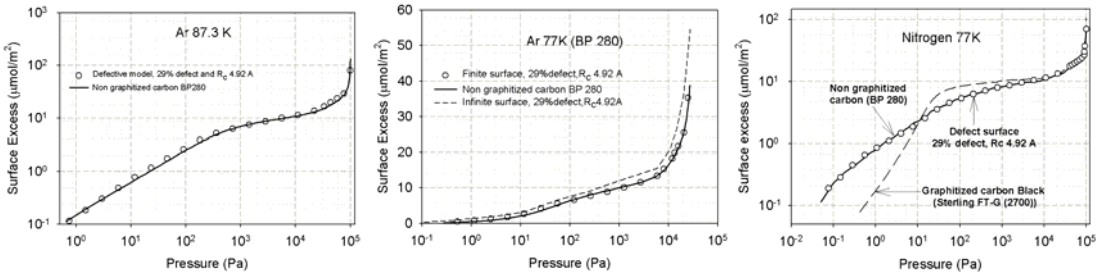

Figure 24 (a) Adsorption isotherm of argon at 87.3 K for BP 280 and the GCMC results (solid line); **(b)** Adsorption isotherm of argon at 77 k for BP280; **(c)** Adsorption of nitrogen at 77K for BP280

Interestingly we find that the same molecular model with a defect percentage of 29% and a defective radius of 4.92 A can describe the data of argon at 77K and nitrogen at 77K very well, as seen in Figures 24b, c. Thus, this demonstrates that a defect model developed here can describe well adsorption on non-graphitized thermal carbon black. This model has been tested against the data of other non-graphitized carbon blacks, BP460 and BP2000 (Wongkoblap and Do, 2007).

9. Pore Size Distribution

The last point that I would like to present here is the pore size distribution of a solid, and revisit the way how we collect the adsorption data for characterization. Adsorption isotherms obtained from volumetric adsorption experiments are traditionally presented as a plot of excess amount versus pressure. This excess amount is not a direct measured quantity, but rather obtained as the difference between the amount that is introduced into the adsorption cell (N_{dose}) and the amount left in the gas phase (N_{gas}). Thus the excess amount is calculated from the following equation:

$$N_{dose} - N_{gas} = N_{dose} - V_{void}\rho_b \tag{1}$$

The issue of concern here is the second quantity in the above equation. To determine the amount remained in the gas phase, one needs to know the void volume. The helium expansion method is traditionally carried out to obtain the void volume with the assumptions of ideal gas and no adsorption of helium inside the pores. The first assumption is satisfied for helium at ambient conditions, while the second one requires some consideration of the solid under investigation. If the solid contains fine micropores, there is a possibility that helium will adsorb in those pores even at ambient conditions. Another issue associated with this method is that helium may access fine pores that other adsorbates can not. Thus the helium expansion method can over-estimate the void volume. Although helium adsorption can be minimized by conducting experiments at high temperatures, the issue of helium accessibility in small pores that larger adsorbates can not still remains. Thus the helium expansion process leads to an expected, but difficult to quantify, over-estimation of the void volume. What we show below is a new method in which the need for helium expansion experiment is avoided (Birkett and Do, 2006a).

Since the amount introduced into the adsorption cell is known accurately, it is more convenient to collect the adsorption data as the amount introduced into the adsorption cell (N) as a function of equilibrium pressure. This amount introduced into the cell is equal to the sum of the amount in the pores, the amount on the surfaces of large pores as well as on external surfaces and the amount in the void space. Thus, we can write the mass balance equation as:

$$N = m_p \left\{ \int_0^{H^*} [\rho_{av}(P;H)]\, dV + \Gamma(P).S_{ext} \right\} + m_p V' \rho_b \tag{2}$$

where ρ_{av} is the average density in pore of characteristic size H, $\Gamma(p)$ is the surface density and V' is the void volume. The significance of eq. (2) is that the quantity required in the fitting is the amount introduced into the adsorption cell and it is always increasing with pressure. Therefore we do not have any problem with the uncertainty of the maximum in the pore density excess when we deal with supercritical fluids. Since the density in pores, the surface density and the bulk gas density behave differently with P, optimization would give the pore size distribution, the external surface area and the void volume.

As an example, this has been completed using super critical methane at 273.15 K and up to 20 MPa (Birkett and Do, 2006a). The pore size distribution derived from the experiment loading of the adsorption is given in Figure 25a and the resulting fit with experiment data is given in Figure 25b.

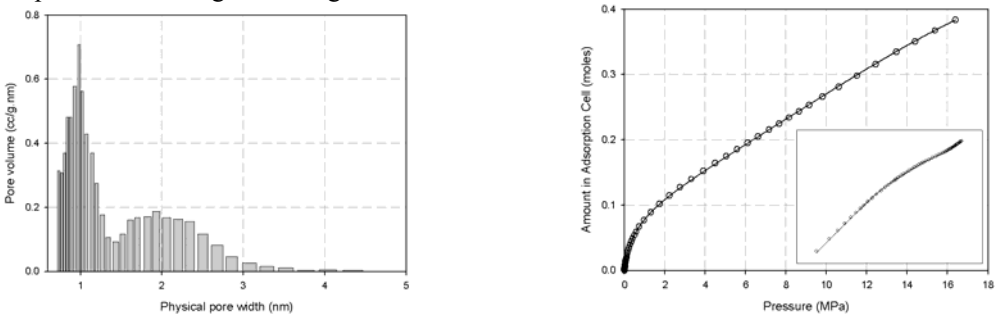

Figure 25. (a) Pore size distribution resulting from the fitting of experimental data at 273.15K.
(b) Amount in adsorption cell at 273.15K, from experiment (O) and simulation (line) using the PSD in (a).

It can be seen from Figure 25 that the fit with experiment is very good and is arrived at without any assumptions made about the accessible volume of the system or the accessible volume of the pore structure. The term V" in Eq. (2) is a fitting term like the pore volume and surface area when it comes to fitting the PSD.

10. Conclusions

In this talk I have presented a general picture about adsorption of simple and complex fluids on simple surfaces such as graphite and in porous solids such as activated carbon. Many aspects of adsorption were presented, and it is clear that more research must done, both theoretically and experimentally to further understand deeply the adsorption mechanism in complex confined space and further develop means to characterize solids in the most unambiguous manner.

Acknowledgement: Support from the Australian Research Council is gratefully acknowledged.

11. References

Avgul, N.N. and A.V. Kiselev. 1970. Physical adsorption of gases and vapors on carbon blacks. *Chem. Phys. Carbon*, 6:1.

Beebe, R.A. and D. M. Young. 1954. Heats of adsorption of argon on a series of carbon blacks graphitized at successive higher temperatures. *J. Phys. Chem.* 58:93.

Birkett, G. and D.D. Do. 2006a. New Method to Determine PSD Using Supercritical Adsorption: Applied to Methane Adsorption in Activated Carbon. *Langmuir* 22:7622.

Birkett, G.R. and D.D. Do. 2006b. Correct Procedures for the Calculation of Heats of Adsorption for Heterogeneous Adsorbents from Molecular Simulation. *Langmuir* 22:9976.

Birkett, G.R. and D.D. Do. 2006c. Simulation study of methanol and ethanol adsorption on graphitized carbon black. *Molecular Simulation* 32:887.

Birkett, G.R. and D.D. Do. 2006c. Ammonia adsorption on graphitized carbon black. *Molecular Simulation* 32:523.

Birkett, G.R. and D.D. Do. 2007a. Simulation study of water adsorption on carbon black: The effect of graphite water interaction strength. *J. Phys. Chem*. (in press)

Do, D.D. and H.D. Do. 2005a. Adsorption of argon on homogeneous graphitized thermal carbon black and heterogeneous carbon surface. *J. Colloid Interface Sci*. 287:452.

Do, D.D. and H.D. Do. 2005b. Effects of potential models in the vapor-liquid equilibria and adsorption of simple gases on graphitized thermal carbon black. *Fluid Phase Equilib*. 236:169.

Do, D.D. and H.D. Do. 2005c. Effects of surface heterogeneity on the adsorption of nitrogen on graphitized thermal carbon black. *Molecular Simulation* 31:651.

Do, D.D. and H.D. Do. 2005d. GCMC-surface area of carbonaceous materials with N2 and Ar adsorption as an alternative to the classical BET method. *Carbon* 43:2112.

Do, D. D. and H. D. Do. 2005e. Adsorption of Flexible n-alkane on Graphitized Thermal Carbon Black. Analysis of Adsorption Isotherm by means of GCMC Simulation, *Chem. Eng. Sci*. 60:1977.

Do, D. D. and H. D. Do. 2005f. Adsorption of quadrupolar, diatomic nitrogen onto graphitized thermal carbon black and in slit shaped carbon pores. *Adsorption Sci. Tech*. 23:267.

Do, D. D. and H. D. Do. 2005g. Adsorption of argon from sub-to supercritical conditions on graphitized thermal carbon black and graphitic slit pores: A Grand canonical Monte Carlo simulation study. *J. Chem. Phys.* 123: 084701.

Do, D.D. and H.D. Do. 2006a. Adsorption of benzene on graphitized thermal carbon black: Reduction of the quadrupole moment in the adsorbed phase. *Langmuir* 22:1121.

Do, D.D. and H.D. Do. 2006b. Adsorption of carbon tetrachloride on graphitized thermal carbon black and in slit graphitic pores: Five-site versus one-site potential models. *J. Phys. Chem. B* 110 ;9520.

Do, D.D. and H.D. Do. 2006c. Modeling of adsorption on nongraphitized carbon surface: GCMC simulation studies and comparison with experimental data. *J. Phys. Chem. B* 110:17531.

Do, D. D.; Do, H. D. 2006d. Evaluation of 1-Site and 5-Site models of methane on its adsorption on graphite and in graphitic slit pores. *J. Phys. Chem. B* 109:19288.

Do, D.D. and H.D. Do. 2007a. Effects of quadrupole moments of graphite surface on adsorption of simple gases on graphitized thermal carbon black. *Colloids and Surfaces, A: Physicochemical and Engineering Aspects* 300:50.

Do, D.D. and H.D. Do. 2007b. Isotherm and Heat of Adsorption in Porous Solids with Defective Pores - Adsorption of argon and nitrogen at 77 K in Saran activated carbon. *Molecular Simulation* (in press).

Do, D.D., H.D. Do and K. Kaneko. 2004. Effect of surface-perturbed intermolecular interaction on adsorption of simple gases on a graphitized carbon surface. *Langmuir* 20:7623.

Gardner, L., M. Kruk and M. Jaroniec. 2001. Reference data for argon adsorption on graphitized and nongraphitized carbon blacks. *J. Phys. Chem. B* 105:12516.

Isirikyan, A. and A.V. Kiselev. 1961. Absolute Adsorption Isotherms of Vapors of Nitrogen, Benzene and N-Hexane, and Heats of Adsorption of Benzene and N-Hexane on Graphitized Carbon Blacks . *J. Phys. Chem.* 65:601.

Murphy, C., K. Singer, M. Klein and I. McDonald. 1980. Pairwise additive effective potentials for nitrogen. *Mol. Phys*. 41:1387.

Olivier JP. 1995. Modeling physical adsorption on porous and nonporous solids using DFT. *J. of Porous Materials* 2(1):9.

Steele, W.A. 1973. Physical interaction of gases with crystalline solids. I. *Surf. Sci*. 36:317.

Wick, C.D., J.I. Siepmann, W.L. Klotz and M.R. Schure. 2002. Temperature effects on the retention of n-alkanes and arenes in helium-squalane gas-liquid chromatography - Experiment and molecular simulation. *Journal of Chromatography A* 954:181.

Wongkobalp, A. and D. D. Do. 2007. Characterization of Cabot non-graphitized carbon blacks with a defective surface model: Adsorption of argon and nitrogen. *Carbon* 45:1527.